

Ultrabroad-band x-ray source using a picosecond, laser-driven plasma accelerator

N. Lemos¹, P. M. King^{1,2}, D. Rusby¹, I. Pagano^{1,2}, M. Sinclair³, K. A. Marsh³, J. L. Shaw⁴,
A. L. Milder⁴, A. Pak¹, B. B. Pollock¹, M. Aufderheide¹, F. V. Hartemann^{1,5}, S. Q. Wu⁶, Y. Hwang⁵,
B. M. Hegelich^{2,6,7}, J. Moody¹, P. Michel¹, C. Joshi³ and F. Albert¹

¹*Lawrence Livermore National Laboratory, NIF and Photon Sciences, 7000 East Avenue, Livermore, California 94550, USA*

²*Department of Physics, University of Texas at Austin, Austin, Texas 78712, USA*

³*Department of Electrical Engineering, University of California Los Angeles, 405 Hilgard Avenue, Los Angeles, California 90095, USA*

⁴*Laboratory for Laser Energetics, University of Rochester, 250 East River Road, Rochester, New York 14623, USA*

⁵*Lumitron Technologies, Incorporated, Irvine, California 92617, USA*

⁶*Center for Relativistic Laser Science, Institute for Basic Science, Gwangju 61005, Korea*

⁷*Department of Physics and Photon Science, GIST, Gwangju 61005, Korea*



(Received 14 May 2023; revised 1 March 2024; accepted 30 May 2024; published 26 July 2024)

An ultrabroad-band x-ray source, with photon energies from 10 keV to >1 MeV, based on a picosecond laser-driven plasma accelerator, is characterized and used to radiograph high-energy-density-science relevant targets. The measured yield of 10^{12} photons/shot is reaching the necessary photon yields to radiograph, in a single shot, high areal density objects and matter under extreme conditions. By focusing a short laser pulse (120 J, 1 ps) into a gas jet, a <100 mrad electron beam with energies up to 350 MeV and up to 70 nC of charge was produced by a combination of laser self-modulation instability and direct laser acceleration. A foil placed at the exit of the gas jet is used to convert part of the electron beam energy into x rays through inverse bremsstrahlung and/or inverse Compton scattering, generating a bright, broad-band, high-photon-energy beam. This beam is used to radiograph a gold half hohlraum with a high-density sphere inside with relevant characteristics for high-energy-density science and inertial confinement fusion.

DOI: [10.1103/PhysRevResearch.6.L032022](https://doi.org/10.1103/PhysRevResearch.6.L032022)

The advent of high-energy density (HED) facilities, in particular high-power lasers and Z pinches, has opened up access to a new regime where temperatures and pressures are comparable to the center of stars and planets [1] and the potential to harness fusion energy through inertial confinement fusion (ICF) [2,3]. In order to probe HED and ICF experiments in the laboratory, a significant flux of high-energy (>1 MeV) photons is required to radiograph high areal density objects with micron spatial resolution and picosecond temporal resolution to avoid motion blurring. Examples include double-shell implosions [4] or flash radiography for diagnosing the hydrodynamics of explosively driven high-atomic-number materials [5]. X-ray probes for radiography in HED and ICF experiments are typically produced from the interaction of a high-power laser with a solid target. At the National Ignition Facility (NIF), time-resolved measurements of the fuel density profile of the stagnation phase of ICF implosions are made using Compton radiography. However, the x-ray source is typically limited to photon energies of 200 keV [6,7]. Other techniques, employing the use of wire microstructures [8], or compound parabolic concentrators targets [9,10] can increase coupling of laser energy into hot

electrons, which can increase both the photon flux and energy into the MeV range. To radiograph complex HED and ICF experiments, an ideal x-ray backlighter should have the ability to produce keV-MeV photon beams with sub-10- μ m spatial and sub-ps temporal resolution.

Within this context, x-ray sources based on electron laser-plasma accelerators (LPAs) [11–15] are potentially attractive as probes in these applications because, unlike conventional laser-produced bremsstrahlung [16–20] or x-ray line radiation sources [21–26], they are highly directional and can resolve μ m size features [12,14,27,28]. The x-ray yield of current x-ray sources based on LPA is limited by the electron beam charge produced when using Joule-class, tens-of-fs duration laser pulses. The use of a ps, kJ-class laser to drive a hybrid LPA that produces relativistic electrons ($\gamma \gg 1$, where γ is the electron Lorentz factor) through a combination of plasma parametric instabilities [29,30] and direct laser acceleration (DLA) [31], has been shown to be a promising platform that produces electron beams with charge up to the microcoulomb range [32,33]. The advantage of using a hybrid LPA is that the electrons that overlap with the laser can get extra energy from DLA. Such electron beams have been used to produce x rays through betatron emission in the tens of keV range [34,35], inverse Compton scattering (ICS) up to 250 keV, and bremsstrahlung beyond 1 MeV [36].

In this Letter, we demonstrate an x-ray source based on a hybrid LPA [37] with an increased x-ray yield of two orders of magnitude over existing x-ray sources based on laser

Published by the American Physical Society under the terms of the [Creative Commons Attribution 4.0 International](https://creativecommons.org/licenses/by/4.0/) license. Further distribution of this work must maintain attribution to the author(s) and the published article's title, journal citation, and DOI.

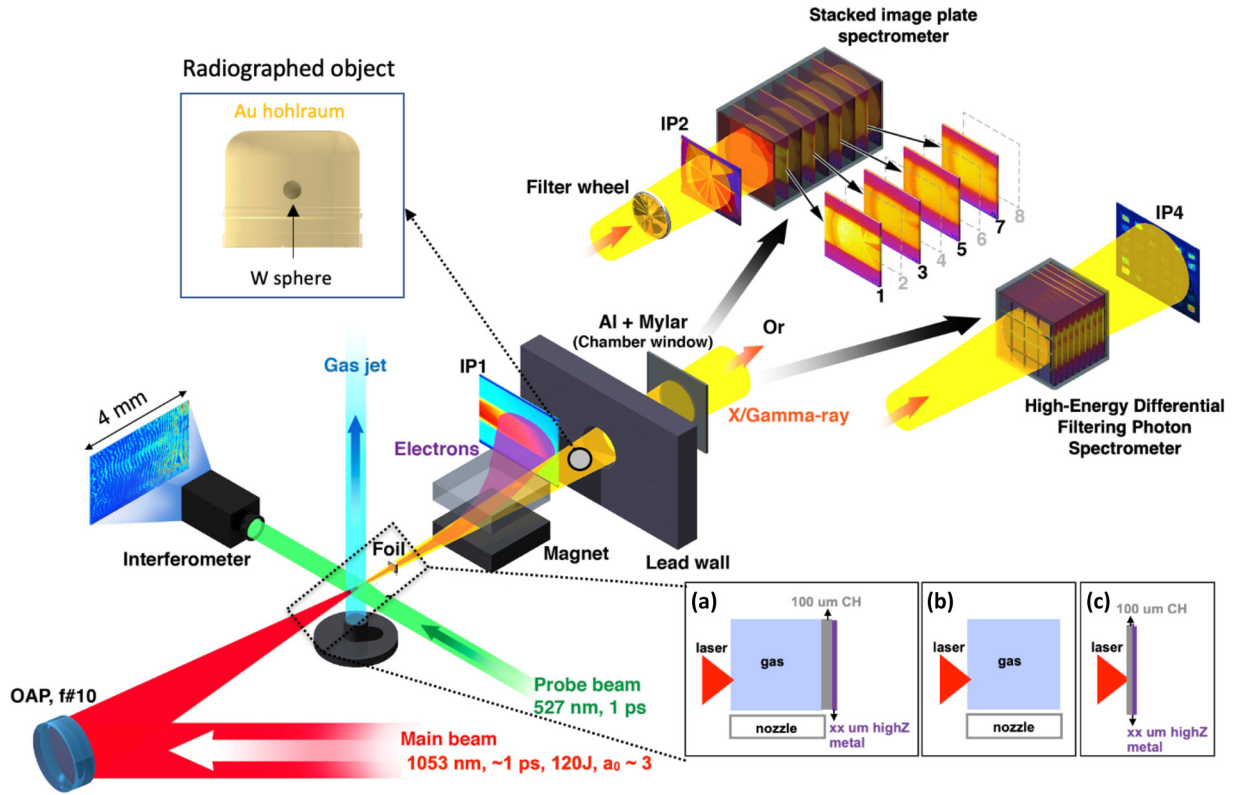


FIG. 1. Experimental setup for generating high-energy x rays from relativistic electrons produced by a hybrid LPA. The Titan laser (red beam with a repetition rate of 60 min) is focused 1 mm into a 10-mm supersonic gas jet and 2 mm from the top of the nozzle. The probe beam (green) crosses the interaction region into a folded wave-front interferometer. A typical interferogram with a field of view large enough to see the full interaction region is shown next to the interferometer. The remaining laser beam and the electrons (pink) collide with a foil to generate a hard x-ray beam (yellow) through ICS and/or bremsstrahlung depending on the foil material. The electrons that cross the foil are dispersed and removed from the laser axis by a magnet and are recorded by an image plate (IP1). The radiographed object (half a hohlraum) is placed on the x-ray beam axis, 50 cm from the gas jet. Three sets of x-ray diagnostics are used (see text for details). The hohlraum radiograph was recorded on IP2 removing the filter wheel. (a) Configuration to generate a x-ray beam with a LWFA + ICS + inverse Bremsstrahlung (IB), (b) configuration to generate a x-ray beam with a LWFA, and (c) a classic laser solid interaction.

wakefield acceleration (LWFA) [27,38] and more than an order of magnitude over the hybrid LPA sources [36], reaching the necessary photon yields to radiograph high areal density objects ($\sim 1 \text{ g/cm}^2$) and matter under extreme conditions [39]. The high yield of ultrabroad-band x rays is due to an increase of $\sim 25\times$ in the total accelerated electron charge. We explore the ICS mechanism [40] and/or inverse bremsstrahlung to maximize the photon yield at different photon energies and we show that this source can be used to radiograph an object with areal density $\sim 1 \text{ g/cm}^2$. For ICS, the accelerated relativistic electrons Compton scatter the nearly head-on colliding laser photons, which on the laboratory frame are Doppler shifted by a factor of $\propto 4\gamma^2$ in a process known as ICS [27,38]. For bremsstrahlung, the accelerated electron beam passes through a high-Z foil that is placed downstream of the hybrid LWFA, converting part of the electron’s energy into x rays through inverse bremsstrahlung.

The experiments were carried out at Lawrence Livermore National Laboratory using the Titan laser system. Figure 1 shows a schematic of the experimental setup and the diagnostics used. The laser pulse has an energy up to 120 J (on target), an average duration of $0.7^{+0.3}_{-0.1}$ ps [full width at half maximum (FWHM)], and a central wavelength of

1053 nm. It is focused by an $f/10$ off-axis parabola (OAP) 1 mm inside a 10-mm-wide column of helium gas emanating from a supersonic nozzle [41,42]. The vacuum spot size, measured at low laser power, is 29 μm ($1/e^2$ intensity point), reaching a peak intensity of $I = 1.1 \times 10^{19} \text{ W/cm}^2$ and a normalized vector potential $a_0 = 3$, with $a_0 = 8.5 \times 10^{-10} \lambda^2 (\mu\text{m}) I (\text{W/cm}^2)$ where λ is the laser wavelength. The electron density in the interaction region is probed using a folded wave-front interferometer [43] that employs a 2-mJ, 1-ps (FWHM) frequency-doubled laser pulse (527 nm). The average measured density of the helium plasma is 10^{18} cm^{-3} . The laser pulse generates relativistic plasma waves through the Raman forward scattering (RFS) and self-modulation (SM) laser instabilities [29,30]. Electrons are accelerated to highly relativistic energies by the longitudinal electric field of the plasma waves and through direct laser acceleration (DLA) [29,44–47] within the plasma waves and in the ion channel that forms behind the plasma waves. DLA is the direct coupling of the transverse electric field of the laser to the electrons undergoing betatron oscillations in the plane of laser polarization. A foil (at 7° with respect to the laser normal) is placed at end of the nozzle (with an uncertainty of $\pm 2 \text{ mm}$) [Fig. 1(a)]. A fraction of the laser energy is absorbed

by the foil creating a surface plasma that acts as a mirror [48]. The plasma mirror reflects the laser photons backwards, where they collide with the high-energy electron beam and generate an x-ray beam via ICS [36] (Fig. 1). The electron beam then propagates through the foil(s) and generates more x rays through inverse bremsstrahlung [36,43]. To maximize the total x-ray yield, a high-Z foil is used to increase x-ray production by inverse bremsstrahlung. Upon traversing the foil(s), the electrons are dispersed onto an image plate (IP1) by a 0.9-T dipole magnet (at 12 cm from the nozzle) in order to characterize the electron beam spectrum and charge and to separate the electron beam from the x-ray beam. To block the background noise generated inside the chamber, a lead wall with an opening of 4 in. \times 6 in. is placed 80 cm after the gas jet. The high-energy x rays exit the chamber through a 12- μ m aluminum and 200- μ m Mylar filter window (4 in. diameter) into the x-ray diagnostics. Outside the vacuum chamber, three different diagnostics are used to characterize the x-ray beam. For x-ray energies between 5 and 30 keV, a filter wheel is used to make differential measurements of transmitted x rays by using ten metallic filter wedges placed in a “Ross pair” arrangement [49] that are recorded by an image plate (IP2). The remaining x-ray signal continues into a stacked-image-plate spectrometer [34,50] that measures x rays with energies between 30 and 100 keV. The higher-energy photons (80 keV–1 MeV) are measured with a high-energy differential-filtering photon spectrometer (HEDFPS) [51], which has an array of 36 different filters of Ta and Al with variable thickness, and are recorded by IP4 that is 30 cm away. The angle covered by any of the three diagnostics was \sim 30 mrad, \sim 2 \times smaller than the divergence of any of the x-ray sources and that of the electron beam. The electron beam energy spectrum, divergence, shape, and charge were first characterized and optimized without any foils to avoid the emittance growth of the electrons (for more information, refer to the Supplemental Material [52]).

The relativistic electrons can generate forward propagating x rays through three principal mechanisms: electron betatron motion inside the LWFA, bremsstrahlung radiation from electrons propagating through a solid density target, and ICS from electrons oscillating inside the laser field—often all these mechanisms are at play in the same experiment [36]. In order to isolate and characterize each mechanism the experimental setup was adjusted by removing or adding a foil(s) or the gas jet as shown in Fig. 1(a) (all mechanisms at play), Fig. 1(b) (only betatron radiation), and Fig. 1(c) (only bremsstrahlung radiation from the laser colliding with the foil) [36]. Figure 2 shows the photon spectra when using the configuration shown in Fig. 1(a) using three different foil configurations: 100 μ m CH foil to test the ICS platform (curves and points in blue), 100 μ m CH + 50 μ m W foils (curves and points in red) and 100 μ m CH + 250 μ m W foil (curves and points in black) to test the electron inverse bremsstrahlung platform. For the ICS platform, a low-Z material is used as a plasma mirror to increase reflectivity and to reduce the bremsstrahlung radiation created by the laser and the electrons hitting the foil [27,53,54]. When using the two foils the idea was to combine both studied sources, pure ICS (using a 100- μ m CH foil), and pure electron bremsstrahlung (thick W foil). The photon energy spectrum was analyzed using three different methods (explained in detail in Ref. [49]) that were applied to each

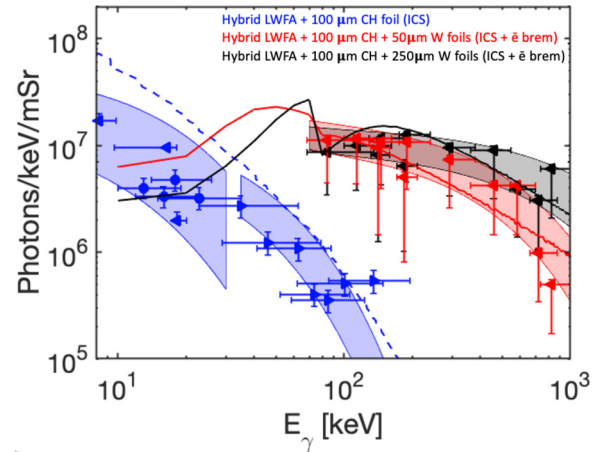


FIG. 2. X-ray energy spectra of the experimental and simulated configurations shown in Fig. 1(a). The blue shaded region and blue points (circles: Ross pairs [49]; triangles: DAT [49]) show the measured x-ray spectrum with a 100- μ m CH foil placed after the nozzle. The dashed blue curve represents the ICS spectrum calculated assuming a collision between an electron beam with the measured experimental characteristics and a laser beam with $a_0 = 1$. The red and black shaded region and red and black points (circles: RP; triangles: DAT) show the measured x-ray spectrum with a 100 μ m CH + 50 μ m W or 100 μ m CH + 250 μ m W foil placed after the nozzle. The solid red and black curves show the respective GEANT4 calculations using an electron beam with the measured experimental characteristics.

of the three diagnostics when possible [36]. When using the ICS platform, at photon energies of 10 keV, the ICS contribution is on the order of the sum of the laser bremsstrahlung and betatron contributions (see Supplemental Material [52] for details). It rapidly becomes larger such that at 40 keV, which is an order of magnitude higher than that due to the sum of the betatron and laser bremsstrahlung mechanisms. This is indicative of the ICS contribution becoming larger at higher energies. To explain the experimental spectrum and yield obtained through ICS, we performed simulations of the ICS mechanism (see Supplemental Material [52] for details). Figure 2 shows a comparison of the simulated ICS spectrum and the experiment. The calculated ICS spectrum fits well with the experimental spectrum, indicating that ICS is the dominating x-ray production mechanism. The total number of photons per shot is \sim 10¹⁰ for photon energies above 10 keV, energy beyond which ICS dominates the spectrum. This value represents an improvement of two orders of magnitude when compared to the ICS LWFA results obtained in the blowout regime [27,38] and is similar to the yield achieved in Ref. [36].

To increase the efficiency of the x-ray source, a second high-Z foil (W) was added so that the high-charge electron beam converts part of its energy into x rays through inverse bremsstrahlung. Since higher-energy x rays are generated in this configuration, the signal was measured with the HEDFPS. As expected, the 250- μ m W foil x-ray spectra (black curve in Fig. 2) has a higher temperature (see Supplemental Material [52]) and photon yield for higher photon energies, when compared to the 50- μ m W foil (red curve in Fig. 2), since the electron stopping range is better matched to the electron beam

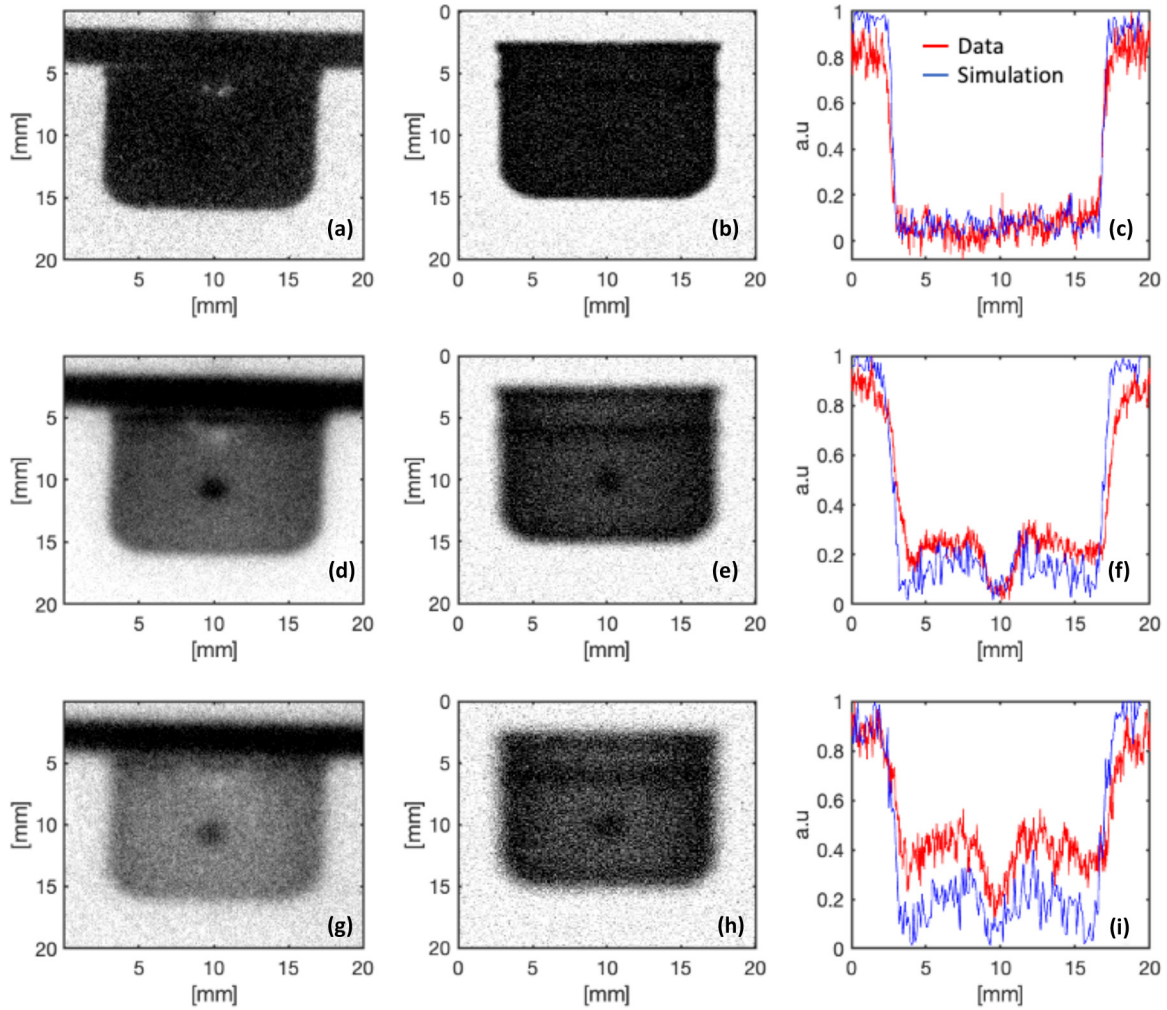


FIG. 3. Hohlräum radiography from (a), (d), (g) experiments and (b), (e), (h) simulation using a 100 μm CH (first row) or 100 μm CH + 50 μm (second row) or 100 μm CH + 250 μm (third row) foil placed after the nozzle. (c), (f), and (i) show the center horizontal lineouts of the experimental (red) and simulated (blue) radiographies for the three types of targets.

energies. When compared to the ICS platform it is possible to see that there is an increase in the photon yield by one order of magnitude at photon energies of 100 keV and of two orders of magnitude at photon energies of 500 keV. This result represents an increased x-ray yield of two orders of magnitude over existing x-ray sources based on LWFA [27,38] and more than one order of magnitude than a hybrid LWFA [36]. It is worth mentioning that most of the ICS produced photons are absorbed by the thick W foil and that here ICS does not contribute to the final spectrum, but using a thinner high-Z foil ($<10 \mu\text{m}$ W, will block 50% at 25 keV) both mechanisms can significantly contribute to the final spectrum. The red and blue solid curves in Fig. 2 show the scaled GEANT4 simulated x-ray spectra using the measured electron experimental parameters (simulation details in the Supplemental Material [52]). These show good agreement with the measured x-ray spectra.

To test the applicability of this source to HEDS, we carried out radiography of a half hohlraum (with 30- μm -thick gold walls) with a 400- μm radius tungsten sphere at the center, which has an areal density of 0.7 g cm^{-2} . As a reference, in an ICF implosion at bang time, the capsule can reach areal

densities just above 1 g cm^{-2} and a radius of 40 μm [7]. Figure 3 shows the experimental (first column) and simulated (second column) radiographies when using the three tested foils after the nozzle. It is possible to see that when only using the ICS only platform (first row), the W sphere inside the hohlraum is not visible. When using the ICS+bremstrahlung source (in this case the dominant x-ray production mechanism is bremsstrahlung since the ICS photons get absorbed by the thick W foil), the W sphere becomes visible, indicating that the last two targets produce more high-energy photons (as shown in Fig. 2). The middle column images show the simulated radiography images using the x-ray source characteristics presented in Fig. 2. The simulated radiographies are generated using the HADES code [55] (more information is given in the Supplemental Material [52]). The simulated radiography shows excellent agreement with the experimental images. This is visible in Figs. 3(c), 3(f), and 3(i), which show normalized lineouts of the experimental (red line) and simulated (blue line) radiographies. In the simulated ICS platform [Fig. 3(b)], if the Gaussian white noise function was not added, the radiograph would show the W sphere inside the

hohlraum. This indicates that if the background noise of the experiment was better mitigated, the ICS source alone would have enough high-energy photons to create contrast between the W sphere and the hohlraum wall. When increasing the W foil thickness from 50 to 250 μm , the contrast of the W sphere and the hohlraum walls is reduced, indicating that the source is generating too many high-energy photons for this radiography target. Thus, for every specific radiography target, there is an optimal W thickness to maximize the radiography contrast. The $1/e^2$ (intensity) source size of the x-ray beam was found to be 140 ± 40 , 280 ± 40 , and 420 ± 50 μm for the images from the top to bottom. The source size was determined using the technique presented in Ref. [56]. The source divergence was measured to be 53×51 mrad ± 10 mrad, $80 \times 90 \pm 20$ mrad, and $60 \times 70 \pm 20$ mrad for the images from the top to bottom. These results show the proof-of-principle application of this x-ray source applied to HEDS and ICF where it can be used to perform Compton radiography [7] of a real implosion.

In conclusion, we have generated an ICS+bremstrahlung x-ray source from a hybrid LPA using a ps laser pulse. The generated x-ray beam has a far greater yield (at energies above

tens of keV that extends beyond 500 keV) than x-ray sources based on LWFA electrons alone. This source promises to be a very useful tool for the study of radiography of high areal density objects and matter under extreme conditions.

This work was performed under the auspices of the U.S. Department of Energy under Contract No. DE-AC52-07NA27344, supported by the Laboratory Directed Research and Development (LDRD) Program under tracking codes 16-ERD-024 at LLNL, and by the joint NNSA/DOE program Grant No. DE-NA0004132 at UCLA. F.A. acknowledges support from the DOE Office of Science Early Career Research Program under SCW1575-1. B.M.H. and P.K. acknowledge support from the Air Force Office of Scientific Research (AFOSR) under Grant No. FA9550-17-1-0264. B.M.H. acknowledges support by the Institute of Basic Science (IBS) under Grant No. IBS-R012-D1. I.P. acknowledges support from DOE/NNSA Grant No. DE-NA0004081 and LLNL-SD ACT-UP Subcontract No. B65092. The authors thank R. C. Cauble, S. Andrews, B. Stuart, R. Costa, C. Bruns, C. Cadwalader, and S. Maricle for their support of the Titan laser system at the Jupiter Laser Facility.

-
- [1] B. A. Remington, High energy density laboratory astrophysics, *Plasma Phys. Controlled Fusion* **47**, A191 (2005).
- [2] J. Lindl, Development of the indirect-drive approach to inertial confinement fusion and the target physics basis for ignition and gain, *Phys. Plasmas* **2**, 3933 (1995).
- [3] A. B. Zylstra, O. A. Hurricane, D. A. Callahan, A. L. Kritcher, J. E. Ralph, H. F. Robey, J. S. Ross, C. V. Young, K. L. Baker, D. T. Casey *et al.*, Burning plasma achieved in inertial fusion, *Nature (London)* **601**, 542 (2022).
- [4] W. S. Varnum, N. D. Delamater, S. C. Evans, P. L. Gobby, J. E. Moore, J. M. Wallace, R. G. Watt, J. D. Colvin, R. Turner, V. Glebov, J. Soures, and C. Stoeckl, Progress toward ignition with noncryogenic double-shell capsules, *Phys. Rev. Lett.* **84**, 5153 (2000).
- [5] T. Goldsack, T. Bryant, P. Beech, S. Clough, G. Cooper, R. Davitt, R. Edwards, N. Kenna, J. McLean, A. Pearce, M. Phillips, K. Pullinger, D. Short, M. Sinclair, K. Thomas, J. Threadgold, M. Williamson, and K. Krushelnick, Multimegavolt multiaxis high-resolution flash x-ray source development for a new hydrodynamics research facility at AWE Aldermaston, *IEEE Trans. Plasma Sci.* **30**, 239 (2002).
- [6] R. Tommasini, S. P. Hatchett, D. S. Hey, C. Iglesias, N. Izumi, J. A. Koch, O. L. Landen, A. J. MacKinnon, C. Sorce, J. A. Delettrez, V. Y. Glebov, T. C. Sangster, and C. Stoeckl, Development of Compton radiography of inertial confinement fusion implosions, *Phys. Plasmas* **18**, 056309 (2011).
- [7] R. Tommasini, O. L. Landen, L. Berzak Hopkins, S. P. Hatchett, D. H. Kalantar, W. W. Hsing, D. A. Alessi, S. L. Ayers, S. D. Bhandarkar, M. W. Bowers, D. K. Bradley, A. D. Conder, J. M. Di Nicola, P. Di Nicola, L. Divol, D. Fittinghoff, G. Gururangan, G. N. Hall, M. Hamamoto, D. R. Hargrove *et al.*, Time-resolved fuel density profiles of the stagnation phase of indirect-drive inertial confinement implosions, *Phys. Rev. Lett.* **125**, 155003 (2020).
- [8] S. Jiang, L. L. Ji, H. Audesirk, K. M. George, J. Snyder, A. Krygier, P. Poole, C. Willis, R. Daskalova, E. Chowdhury, N. S. Lewis, D. W. Schumacher, A. Pukhov, R. R. Freeman, and K. U. Akli, Microengineering laser plasma interactions at relativistic intensities, *Phys. Rev. Lett.* **116**, 085002 (2016).
- [9] A. G. MacPhee, D. Alessi, H. Chen, G. Cochran, M. R. Hermann, D. H. Kalantar, A. J. Kemp, S. M. Kerr, A. J. Link, T. Ma, A. J. Mackinnon, D. A. Mariscal, D. Schlossberg, R. Tommasini, S. Vohnof, C. C. Widmayer, S. C. Wilks, G. J. Williams, W. H. Williams, and K. Youngblood, Enhanced laser-plasma interactions using non-imaging optical concentrator targets, *Optica* **7**, 129 (2020).
- [10] D. R. Rusby, P. M. King, A. Pak, N. Lemos, S. Kerr, G. Cochran, I. Pagano, A. Hannasch, H. Quevedo, M. Spinks, M. Donovan, A. Link, A. Kemp, S. C. Wilks, G. J. Williams, M. J.-E. Manuel, Z. Gavin, A. Haid, F. Albert, M. Aufderheide *et al.*, Enhancements in laser-generated hot-electron production via focusing cone targets at short pulse and high contrast, *Phys. Rev. E* **103**, 053207 (2021).
- [11] F. Albert and A. G. R. Thomas, Applications of laser wake-field accelerator-based light sources, *Plasma Phys. Controlled Fusion* **58**, 103001 (2016).
- [12] S. Corde, K. Ta Phuoc, G. Lambert, R. Fitour, V. Malka, A. Rousse, A. Beck, and E. Lefebvre, Femtosecond x rays from laser-plasma accelerators, *Rev. Mod. Phys.* **85**, 1 (2013).
- [13] E. Esarey, B. A. Shadwick, P. Catravas, and W. P. Leemans, Synchrotron radiation from electron beams in plasma-focusing channels, *Phys. Rev. E* **65**, 056505 (2002).
- [14] Y. Glinec, J. Faure, L. L. Dain, S. Darbon, T. Hosokai, J. J. Santos, E. Lefebvre, J. P. Rousseau, F. Burgy, B. Mercier, and V. Malka, High-resolution γ -ray radiography produced by a laser-plasma driven electron source, *Phys. Rev. Lett.* **94**, 025003 (2005).

- [15] F. Albert, Principles and applications of x-ray light sources driven by laser wakefield acceleration, *Phys. Plasmas* **30**, 050902 (2023).
- [16] C. Courtois, R. Edwards, A. Compant La Fontaine, C. Aedy, S. Bazzoli, J. L. Bourgade, J. Gazave, J. M. Lagrange, O. Landoas, L. L. Dain, D. Mastrosimone, N. Pichoff, G. Pien, and C. Stoeckl, Characterization of a MeV bremsstrahlung x-ray source produced from a high intensity laser for high areal density object radiography, *Phys. Plasmas* **20**, 083114 (2013).
- [17] M. D. Perry, J. A. Sefcik, T. Cowan, S. Hatchett, A. Hunt, M. Moran, D. Pennington, R. Snavely, and S. C. Wilks, Hard x-ray production from high intensity laser solid interactions (invited), *Rev. Sci. Instrum.* **70**, 265 (1999).
- [18] P. A. Norreys, M. Santala, E. Clark, M. Zepf, I. Watts, F. N. Beg, K. Krushelnick, M. Tatarakis, A. E. Dangor, X. Fang, P. Graham, T. McCanny, R. P. Singhal, K. W. D. Ledingham, A. Creswell, D. C. W. Sanderson, J. Magill, A. Machacek, J. S. Wark, R. Allott *et al.*, Observation of a highly directional γ -ray beam from ultrashort, ultraintense laser pulse interactions with solids, *Phys. Plasmas* **6**, 2150 (1999).
- [19] S. P. Hatchett, C. G. Brown, T. E. Cowan, E. A. Henry, J. S. Johnson, M. H. Key, J. A. Koch, A. B. Langdon, B. F. Lasinski, R. W. Lee, A. J. Mackinnon, D. M. Pennington, M. D. Perry, T. W. Phillips, M. Roth, T. C. Sangster, M. S. Singh, R. A. Snavely, M. A. Stoyer, S. C. Wilks *et al.*, Electron, photon, and ion beams from the relativistic interaction of petawatt laser pulses with solid targets, *Phys. Plasmas* **7**, 2076 (2000).
- [20] J. C. Fernández, D. Cort Gautier, C. Huang, S. Palaniyappan, B. J. Albright, W. Bang, G. Dyer, A. Favalli, J. F. Hunter, J. Mendez, M. Roth, M. Swinhoe, P. A. Bradley, O. Deppert, M. Espy, K. Falk, N. Guler, C. Hamilton, B. M. Hegelich, D. Henzlova *et al.*, Laser-plasmas in the relativistic-transparency regime: Science and applications, *Phys. Plasmas* **24**, 056702 (2017).
- [21] J. D. Hares, J. D. Kilkenny, M. H. Key, and J. G. Lunney, Measurement of fast-electron energy spectra and preheating in laser-irradiated targets, *Phys. Rev. Lett.* **42**, 1216 (1979).
- [22] H. Chen, B. Soom, B. Yaakobi, S. Uchida, and D. D. Meyerhofer, Hot-electron characterization from $K\alpha$ measurements in high-contrast, p -polarized, picosecond laser-plasma interactions, *Phys. Rev. Lett.* **70**, 3431 (1993).
- [23] A. Rouse, P. Audebert, J. P. Geindre, F. Fallières, J. C. Gauthier, A. Mysyrowicz, G. Grillon, and A. Antonetti, Efficient $K\alpha$ x-ray source from femtosecond laser-produced plasmas, *Phys. Rev. E* **50**, 2200 (1994).
- [24] A. B. Sefkow, G. R. Bennett, M. Geissel, M. Schollmeier, B. C. Franke, and B. W. Atherton, Efficiency enhancement for $K\alpha$ x-ray yields from laser-driven relativistic electrons in solids, *Phys. Rev. Lett.* **106**, 235002 (2011).
- [25] H. S. Park, D. M. Chambers, H. K. Chung, R. J. Clarke, R. Eagleton, E. Giraldez, T. Goldsack, R. Heathcote, N. Izumi, M. H. Key, J. A. King, J. A. Koch, O. L. Landen, A. Nikroo, P. K. Patel, D. F. Price, B. A. Remington, H. F. Robey, R. A. Snavely, D. A. Steinman *et al.*, High-energy $K\alpha$ radiography using high-intensity, short-pulse lasers, *Phys. Plasmas* **13**, 056309 (2006).
- [26] B. Westover, A. MacPhee, C. Chen, D. Hey, T. Ma, B. Maddox, H. S. Park, B. Remington, and F. N. Beg, Study of silver $K\alpha$ and bremsstrahlung radiation from short-pulse laser-matter interactions with applications for x-ray radiography, *Phys. Plasmas* **17**, 082703 (2010).
- [27] K. T. Phuoc, S. Corde, C. Thauray, V. Malka, A. Tafzi, J. P. Goddet, R. C. Shah, S. Sebban, and A. Rouse, All-optical Compton gamma-ray source, *Nat. Photonics* **6**, 308 (2012).
- [28] S. Kneip, C. McGuffey, J. L. Martins, S. F. Martins, C. Bellei, V. Chvykov, F. Dollar, R. Fonseca, C. Huntington, G. Kalintchenko, A. Maksimchuk, S. P. D. Mangles, T. Matsuoaka, S. R. Nagel, C. A. J. Palmer, J. Schreiber, K. T. Phuoc, A. G. R. Thomas, V. Yanovsky, L. O. Silva *et al.*, Bright spatially coherent synchrotron x-rays from a table-top source, *Nat. Phys.* **6**, 980 (2010).
- [29] A. Modena, Z. Najmudin, A. Dangor, C. Clayton, K. Marsh, C. Joshi, V. Malka, C. Darrow, C. Danson, D. Neely, and F. Walsh, Electron acceleration from the breaking of relativistic plasma-waves, *Nature (London)* **377**, 606 (1995).
- [30] C. Joshi, T. Tajima, J. M. Dawson, H. A. Baldis, and N. A. Ebrahim, Forward Raman instability and electron acceleration, *Phys. Rev. Lett.* **47**, 1285 (1981).
- [31] A. Pukhov, Z.-M. Sheng, and J. Meyer-ter-Vehn, Particle acceleration in relativistic laser channels, *Phys. Plasmas* **6**, 2847 (1999).
- [32] J. Shaw, M. Romo-Gonzalez, N. Lemos *et al.*, Microcoulomb ($0.7 \pm \frac{0.4}{0.2}$ μC) laser plasma accelerator on OMEGA EP, *Sci. Rep.* **11**, 7498 (2021).
- [33] P. M. King, K. Miller, N. Lemos, J. L. Shaw, B. F. Kraus, M. Thibodeau, B. M. Hegelich, J. Hinojosa, P. Michel, C. Joshi, K. A. Marsh, W. Mori, A. Pak, A. G. R. Thomas, and F. Albert, Predominant contribution of direct laser acceleration to high-energy electron spectra in a low-density self-modulated laser wakefield accelerator, *Phys. Rev. Accel. Beams* **24**, 011302 (2021).
- [34] F. Albert, N. Lemos, J. L. Shaw, B. B. Pollock, C. Goyon, W. Schumaker, A. M. Saunders, K. A. Marsh, A. Pak, J. E. Ralph, J. L. Martins, L. D. Amorim, R. W. Falcone, S. H. Glenzer, J. D. Moody, and C. Joshi, Observation of betatron x-ray radiation in a self-modulated laser wakefield accelerator driven with picosecond laser pulses, *Phys. Rev. Lett.* **118**, 134801 (2017).
- [35] S. Kneip, N. S. R., C. Bellei, N. Bourgeois, A. E. Dangor, A. Gopal, R. Heathcote, S. P. D. Mangles, J. R. Marques, A. Maksimchuk, P. M. Nilson, K. T. Phuoc, S. Reed, M. Tzoufras, F. S. Tsung, L. Willingale, W. B. Mori, A. Rouse, K. Krushelnick, and Z. Najmudin, Observation of synchrotron radiation from electrons accelerated in a petawatt-laser-generated plasma cavity, *Phys. Rev. Lett.* **100**, 105006 (2008).
- [36] N. Lemos, P. King, J. L. Shaw, A. L. Milder, K. A. Marsh, A. Pak, B. B. Pollock, C. Goyon, W. Schumaker, A. M. Saunders, D. Papp, R. Polanek, J. E. Ralph, J. Park, R. Tommasini, G. J. Williams, H. Chen, F. V. Hartemann, S. Q. Wu, S. H. Glenzer *et al.*, X-ray sources using a picosecond laser driven plasma accelerator, *Phys. Plasmas* **26**, 083110 (2019).
- [37] N. Lemos, J. L. Martins, F. S. Tsung, J. L. Shaw, K. A. Marsh, F. Albert, B. B. Pollock, and C. Joshi, Self-modulated laser wakefield accelerators as x-ray sources, *Plasma Phys. Controlled Fusion* **58**, 034018 (2016).
- [38] N. D. Powers, I. Ghebregziabher, G. Golovin, C. Liu, S. Chen, S. Banerjee, J. Zhang, and D. P. Umstadter, Quasi-monoenergetic and tunable x-rays from a laser-driven Compton light source, *Nat. Photonics* **8**, 28 (2014).

- [39] G. R. Bennett, M. E. Cuneo, R. A. Vesey, J. L. Porter, R. G. Adams, R. A. Aragon, J. A. Caird, O. L. Landen, P. K. Rambo, D. C. Rovang, L. E. Ruggles, W. W. Simpson, I. C. Smith, and D. F. Wenger, Symmetric inertial-confinement-fusion-capsule implosions in a double-Z-pinch-driven hohlraum, *Phys. Rev. Lett.* **89**, 245002 (2002).
- [40] F. V. Hartemann, *High-Field Electrodynamics* (CRC Press, Boca Raton, FL, 2001).
- [41] N. Lemos, N. Lopes, J. M. Dias, and F. Viola, Design and characterization of supersonic nozzles for wide focus laser-plasma interactions, *Rev. Sci. Instrum.* **80**, 103301 (2009).
- [42] S. Semushin and V. Malka, High density gas jet nozzle design for laser target production, *Rev. Sci. Instrum.* **72**, 2961 (2001).
- [43] N. Lemos, L. Cardoso, J. Geada, G. Figueira, F. Albert, and J. M. Dias, Guiding of laser pulses in plasma waveguides created by linearly-polarized femtosecond laser pulses, *Sci. Rep.* **8**, 3165 (2018).
- [44] J. L. Shaw, N. Lemos, L. D. Amorim, N. Vafaei-Najafabadi, K. A. Marsh, F. S. Tsung, W. B. Mori, and C. Joshi, Role of direct laser acceleration of electrons in a laser wakefield accelerator with ionization injection, *Phys. Rev. Lett.* **118**, 064801 (2017).
- [45] J. L. Shaw, F. S. Tsung, N. Vafaei-Najafabadi, K. A. Marsh, N. Lemos, W. B. Mori, and C. Joshi, Role of direct laser acceleration in energy gained by electrons in a laser wakefield accelerator with ionization injection, *Plasma Phys. Controlled Fusion* **56**, 084006 (2014).
- [46] X. Zhang, V. N. Khudik, and G. Shvets, Synergistic laser-wakefield and direct-laser acceleration in the plasma-bubble regime, *Phys. Rev. Lett.* **114**, 184801 (2015).
- [47] S. P. D. Mangles, B. R. Walton, M. Tzoufras, Z. Najmudin, R. J. Clarke, A. E. Dangor, R. G. Evans, S. Fritzler, A. Gopal, C. Hernandez-Gomez, W. B. Mori, W. Rozmus, M. Tatarakis, A. G. R. Thomas, F. S. Tsung, M. S. Wei, and K. Krushelnick, Electron acceleration in cavitated channels formed by a petawatt laser in low-density plasma, *Phys. Rev. Lett.* **94**, 245001 (2005).
- [48] G. Doumy, F. Quéré, O. Gobert, M. Perdrix, P. Martin, P. Audebert, J. C. Gauthier, J. P. Geindre, and T. Wittmann, Complete characterization of a plasma mirror for the production of high-contrast ultraintense laser pulses, *Phys. Rev. E* **69**, 026402 (2004).
- [49] P. M. King, N. Lemos, J. L. Shaw, A. L. Milder, K. A. Marsh, A. Pak, B. M. Hegelich, P. Michel, J. Moody, C. Joshi, and F. Albert, X-ray analysis methods for sources from self-modulated laser wakefield acceleration driven by picosecond lasers, *Rev. Sci. Instrum.* **90**, 033503 (2019).
- [50] C. D. Chen, J. A. King, M. H. Key, K. U. Akli, F. N. Beg, H. Chen, R. R. Freeman, A. Link, A. J. Mackinnon, A. G. MacPhee, P. K. Patel, M. Porkolab, R. B. Stephens, and L. D. Van Woerkom, A Bremsstrahlung spectrometer using k -edge and differential filters with image plate dosimeters, *Rev. Sci. Instrum.* **79**, 10E305 (2008).
- [51] G. J. Williams, R. Tommasini, N. Lemos, J. Park, and H. Chen, High-energy differential-filtering photon spectrometer for ultraintense laser-matter interactions, *Rev. Sci. Instrum.* **89**, 10F116 (2018).
- [52] See Supplemental Material at <http://link.aps.org/supplemental/10.1103/PhysRevResearch.6.L032022> for the electron beam and x-ray beams characterization as well as the details about the radiography simulations.
- [53] C. Yu, R. Qi, W. Wang, J. Liu, W. Li, C. Wang, Z. Zhang, J. Liu, Z. Qin, M. Fang, K. Feng, Y. Wu, Y. Tian, Y. Xu, F. Wu, Y. Leng, X. Weng, J. Wang, F. Wei, Y. Yi *et al.*, Ultrahigh brilliance quasi-monochromatic MeV γ -rays based on self-synchronized all-optical Compton scattering, *Sci. Rep.* **6**, 29518.
- [54] H.-E. Tsai, X. Wang, J. Shaw, A. V. Arefiev, Z. Li, X. Zhang, R. Zgadzaj, W. Henderson, V. Khudik, G. Shvets, and M. C. Downer, Compact tunable Compton x-ray source from laser wakefield accelerator and plasma mirror, *Phys. Plasmas* **22**, 023106 (2015).
- [55] M. Aufderheide, G. Henderson, A. von Wittenau, D. Slone, and H. Martz, HADES a code for simulating a variety of radiographic techniques, in *IEEE Symposium Conference Record Nuclear Science 2004* (IEEE, New York, 2004), Vol. 4, pp. 2579–2583.
- [56] I. Pagano *et al.* (unpublished).